Available online at www.sciencedirect.com
ScienceDirect
Journal of Sound and Vibration 320 (2009) 201–220
JOURNAL OF SOUND AND VIBRATION
www.elsevier.com/locate/jsvi

Experimental and numerical analysis of a composite bridge for high-speed trains

K. Liu*, E. Reynders, G. De Roeck, G. Lombaert

Department of Civil Engineering, K.U. Leuven, Kasteelpark, Arenberg 40, B-3001 Leuven, Belgium

Received 3 March 2008; received in revised form 23 May 2008; accepted 15 July 2008
Handling Editor: C.L. Morfey
Available online 29 August 2008

Abstract

This paper presents the in situ dynamic measurements and the experimental validation of the numerical model for the prediction of high-speed train-induced vibration. The Sesia viaduct is considered, which is a composite railway bridge consisted by seven spans. The responses of the bridge are measured both under ambient vibration and under the excitation of Italian ETR500Y high-speed trains. From the modal analysis of the ambient vibration data, two types of mode shapes are identified by operational modal analysis. Based on the dynamic behavior of the adjacent spans, the modes of the bridge can be distinguished as symmetrical and anti-symmetrical patterns, which indicates that although each span is statically decoupled, the ballast and the rails realize a connection between the adjacent spans of the bridge.

To predict the bridge response due to the passage of high-speed trains, two numerical models are considered. First, a train–bridge interaction model for a vehicle system with 15 degrees of freedom is implemented. Second, the train is modeled as a series of moving load. The numerical simulation is validated by comparing the predicted accelerations and strains with measured results, Both models give a good correspondence between the predicted and the measured response. This study provides a better understanding of the structural behavior of a composite railway bridge under the excitation of high-speed trains.

1. Introduction

Steel–concrete composite bridges have been more and more exploited in new lines of the European high-speed railway network due to considerable advantages regarding the design, construction time, durability and costs. Nevertheless, these new design solutions, which have been introduced during a period of quick expansion of the network, amplified problems related to dynamic effects and interaction phenomena, fatigue loading, structural modeling, fatigue life and damage assessment [1].

Frýba [2] is the first to consider the case of beam structures subjected to a moving load. Zhang [3] evaluated the load-carrying capacity of existing composite bridges under a pair of concentrated moving forces. Yang [4] modeled the train as series of moving loads to investigate the key parameters that govern the dynamic

*Corresponding author. Tel.: +32 16 32 16 77; fax: +32 16 32 19 88.
E-mail address: kai.liu@bwk.kuleuven.be (K. Liu).

0022-460X/$ - see front matter Crown Copyright © 2008 Published by Elsevier Ltd. All rights reserved.
doi:10.1016/j.jsv.2008.07.010

responses of the beams. De Roeck [5] predicted the dynamic response of the bridge using moving load model and validated by in situ vibration measurements.

During the last decades considerable experimental and theoretical research on train–bridge interaction has been carried out [6]. The train–bridge interaction model incorporates subsystems for the train and the bridge. The governing equation of motion of the vehicle subsystem is usually derived using Lagrange equation of motion while the coupled train–bridge interaction system is solved using Newmark-β method [7–10]. Based on that, Xia [11] has proposed a dynamic interaction model of the bridge–articulated train system, the vehicle model is a system with 15 degrees of freedom (dof's). The case of the Thalys articulated train passing along the Antoing Bridge on the Paris–Brussels high-speed railway line is analyzed. The dynamic responses of the bridge and the articulated vehicles are calculated and experimentally measured. The proposed analysis model and the solution method are verified through the comparison between the calculated results and the in situ measured data.

The EC research project "DETAILS" aims at the improvement of design, safety and durability of steel–concrete composite bridges. In order to achieve these objectives, structural modeling will be intergraded with experimental tests and health monitoring in order to obtain necessary information on actual bridge loading, structural modeling, fatigue resistance and damage assessment of these types of bridges. As part of the experiments of the project, the Italian Sesia viaduct is tested under ambient vibration and the excitation of Italian ETR500Y high-speed trains.

This paper presents the dynamic experiments and the experimental validation of two approaches for the prediction of the bridge response due to the passage of the high-speed train. It is organized in the following manner. Section 2 presents the dynamic experiments conducted at the Sesia viaduct and the modal analysis based on the measured vibration data. Two types of mode shapes are identified by operational modal analysis from the modal analysis of the ambient vibration data. Based on the dynamic behavior of the adjacent spans, the modes of the bridge can be distinguished as symmetrical and anti-symmetrical patterns. Section 3 describes the numerical model developed for the Sesia viaduct. Emphasis has been given on how to apply appropriate boundary conditions according to the modal properties identified from the experiments. In Sections 4 and 5, two different approaches for predicting the bridge responses due to the train passages are adopted. The numerical simulation is validated by comparing the predicted and the measured response.

2. Experiment on the Sesia viaduct

2.1. Introduction to the bridge

The Sesia viaduct, located on the new Italian high-speed line between Torino and Milano, is a composite railway bridge by seven spans, of 46 m, and has a total length of 322 m (Fig. 1). Each simply supported span

Fig. 1. Global view of the Sesia viaduct.

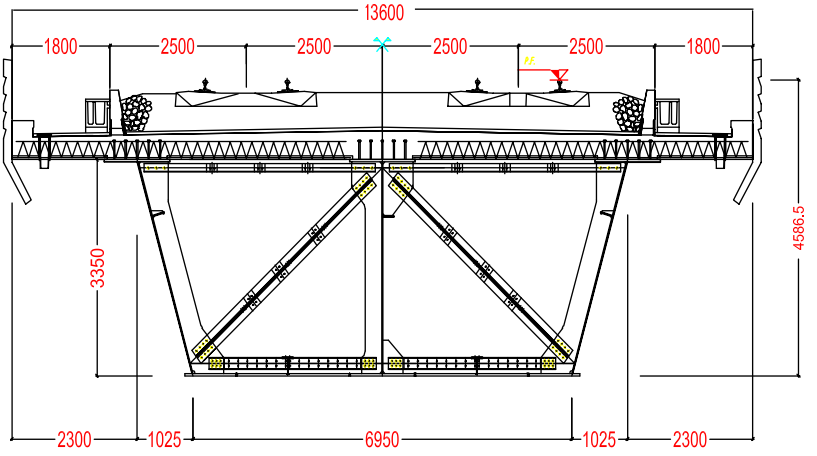

Fig. 2. Cross section of the Sesia viaduct.

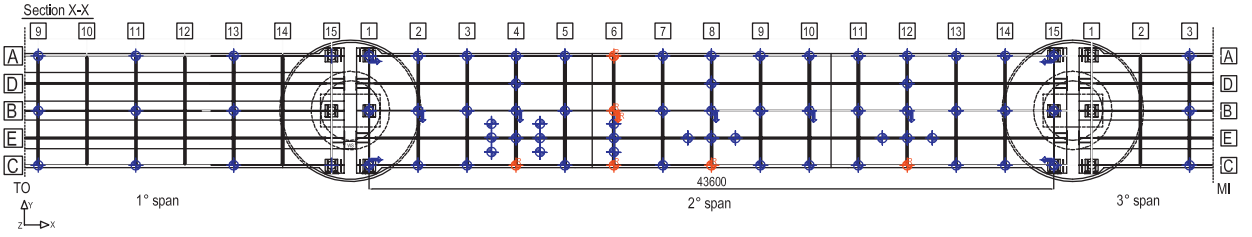

Fig. 3. Global vertical layout.

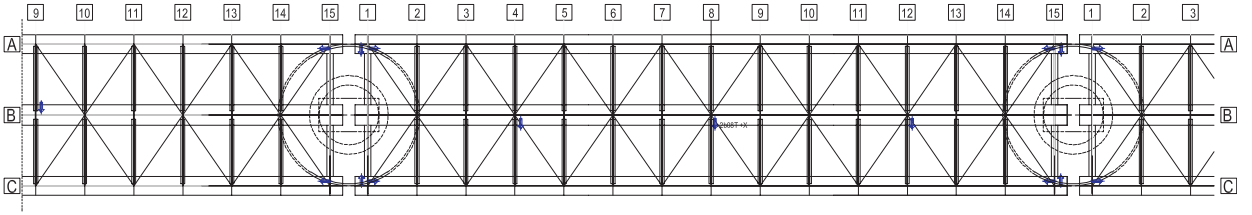

Fig. 4. Global horizontal layout.

consists of a girder of the same double box cross section (Fig. 2). The bottom steel box is composed by lower flanges and three webs. The concrete slab has a width of 13.6 m, a thickness of 0.4 m, and is connected to the steel girder by studs. The total mass of each span is about 1380 ton.

2.2. Measurement setup

The sensor layout is chosen such that global and local structural behavior can be analyzed in both vertical and horizontal directions. Because of the large extension of the bridge, only the second span from Torino to Milano side is extensively tested, both under ambient vibration and the excitation of Italian ETR500Y high-speed trains. Accelerations and strains at different points on the bridge are measured. A small number of sensors are placed on the first and the third span as well to evaluate the dynamic coupling between two neighboring spans. The layouts of accelerometers are shown in Figs. 3 and 4. All measurement channels are denoted by a label $xYzzF$, where the number x denotes the number of the span (1, 2 or 3), the character Y indicates the main girder (A, B or C) or stiffener (D or E), the number zz denotes the number of the section (1–15), and the character F denotes the direction (X, Y or Z).

The local strain field in longitudinal direction is measured with fiber optic sensors of SMARTEC (Fig. 5). These sensors measure the relative displacement between two points, at an intermediate distance of 1 or 1.2 m apart. These measurements are carried out on two cross sections: one next to the pier and another at a quarter of the span (Figs. 6 and 7). A total of eight sensors are placed at four different levels on two vertical lines in order to measure the local strains in the bottom and upper part of the cross section.

Fig. 5. Installation of SOFO sensors.

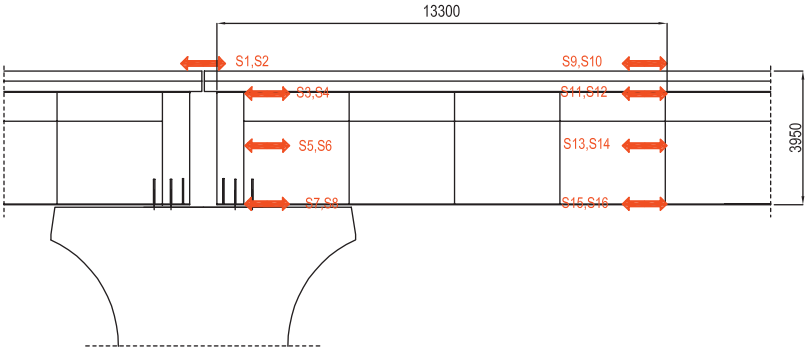

Fig. 6. Vertical view of local strain layout.

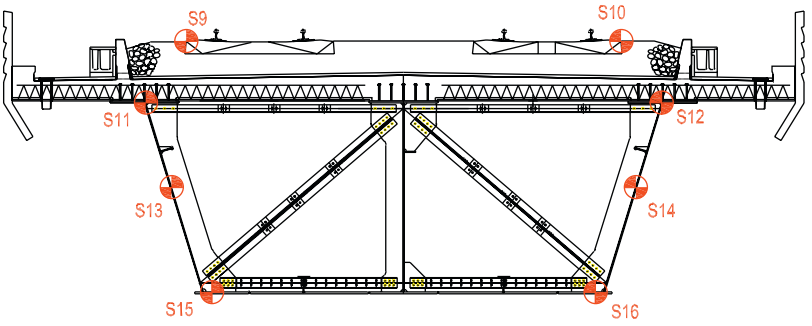

Fig. 7. Local strain layout at a quarter section.

2.3. Modal analysis

The modal analysis is performed using ambient vibration data, free vibration data and train passage data, respectively. A modal model of the bridge is identified using reference-based stochastic subspace identification (SSI) [12]. From the modal analysis of ambient vibration data, a total of eight modes is extracted (Table 1). Based on the dynamic behavior of the adjacent spans, the modes of the bridge can be approximately distinguished as symmetrical and anti-symmetrical patterns (Fig. 8). This indicates that although each span is statically decoupled, the ballast and the rails realize a connection between the adjacent spans that is clearly reflected in the dynamic properties of the bridge.

From the modal analysis of the free vibration data, immediately after the train leaves the considered second span, three modes are identified which correspond to the symmetrical modes, the second torsional mode is not identified (Fig. 9). The first and the second symmetrical bending modes are identified from the modal analysis

Table 1
Identified eigenfrequencies and damping ratios from ambient measurements

Modes	Symmetrical		Anti-symmetrical	
	Frequency (Hz)	Damping ratio ξ (%)	Frequency (Hz)	Damping ratio ξ (%)
First vertical bending mode	4.14	2.17	3.62	1.70
First torsional mode	9.00	1.84	8.35	1.79
Second vertical bending mode	10.44	2.64	10.00	1.84
Second torsional mode	14.28	1.69	11.26	2.20

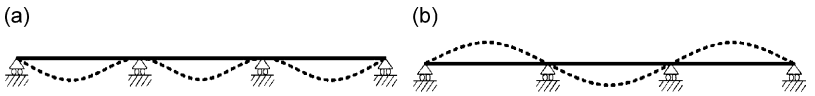

Fig. 8. Identified modes: (a) symmetrical and (b) anti-symmetrical.

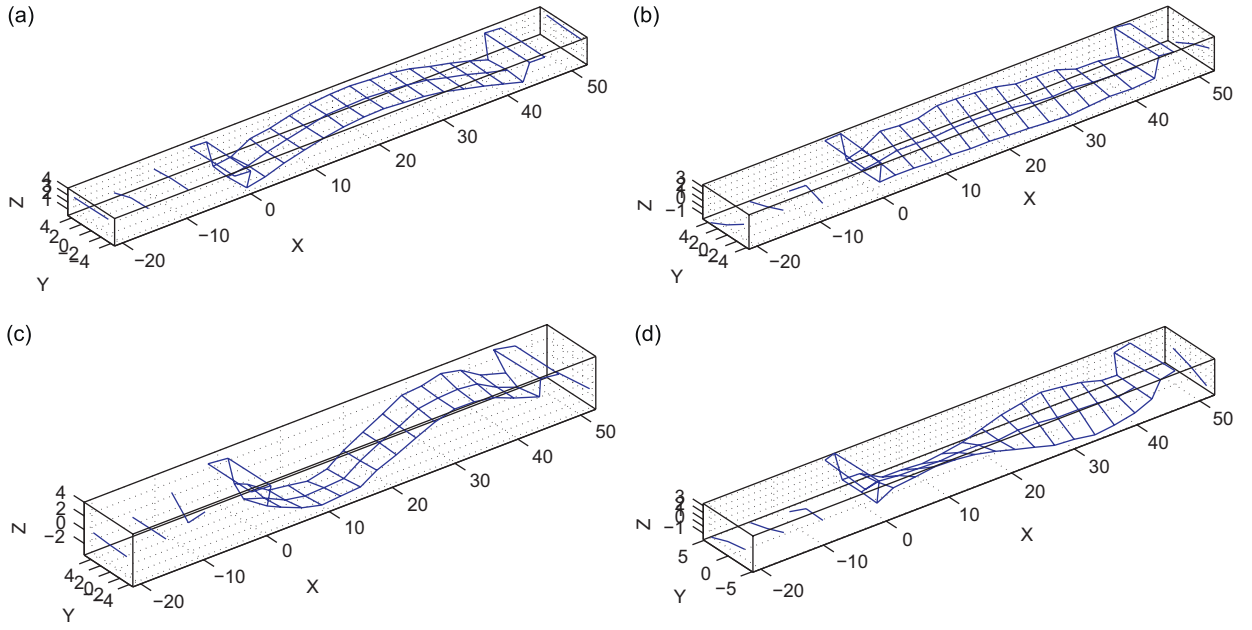

Fig. 9. Identified mode shapes of symmetrical model: (a) first vertical bending mode at 4.14 Hz, (b) first torsional mode at 9.00 Hz, (c) second vertical bending mode at 10.44 Hz and (d) second torsional mode at 14.28 Hz.

Table 2
Comparison of identified eigenfrequencies from different vibration data

Mode	Free vibration		Train forced vibration		Ambient vibration	
	Frequency (Hz)	Damping ratio ξ (%)	Frequency (Hz)	Damping ration ξ (%)	Frequency (Hz)	Damping ration ξ (%)
First vertical bending mode	3.90	2.30	3.67	2.81	4.14	2.17
First torsional mode	9.13	1.25	–	–	9.00	1.84
Second vertical bending mode	10.41	2.38	10.54	4.27	10.44	2.64

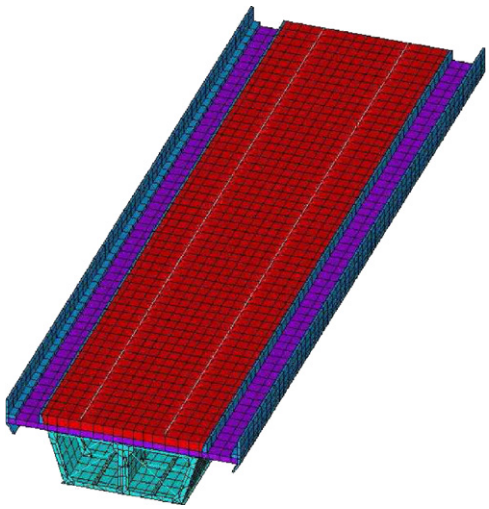

Fig. 10. Numerical model of Sesia viaduct.

of the train passage data. This indicates that symmetrical modes are predominantly excited when the train passes the bridge. Table 2 compares the eigenfrequencies identified from different vibration data, it can be observed that the first bending frequency decreases when the train is on the bridge. This can be due to the mass of the train and the train–bridge interaction, which will be discussed in Section 4.

3. Numerical modeling of the Sesia viaduct

The numerical model (Fig. 10) of the Sesia viaduct is created with the finite element program Ansys. As described in Section 2.3, the symmetrical modes are predominantly excited when the train passes the bridge, appropriate boundary conditions are applied according to the symmetrical modal properties derived from the ambient vibration data. The longitudinal direction of the rail and the ballast are restricted to simulate their continuity (Fig. 11). The element types and material properties are presented in Table 3. Particularly, a linear spring element (combin14) is chosen to represent the headed shear stud. The corresponding nodes of the concrete slab and steel girder are connected by these spring elements in the longitudinal direction and coupled in other directions [13]. The characteristic of the spring element is defined by the load–slip curves obtained from stud push-out tests [14].

The calculated eigenfrequencies are compared to the frequencies of symmetrical modes identified from the ambient vibration data (Table 4). There is a good correspondence between the calculated and measured results.

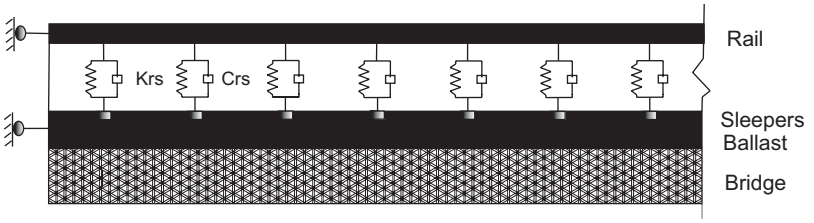

Fig. 11. Track-ballast model.

Table 3
Element types and material characteristics of numerical model

	Element type	E (N/m^2)	ρ (kg/m^3)	v	Mass (kg)	Stiffness (N/m)	Damping (N s/m)
Steel box	shell63	2.056E+11	7850	0.3	–	–	–
Ballast	solid45	2.8E+08	1700	0.28	–	–	–
Concrete slab	solid45	3.1E+10	2500	0.17	–	–	–
Stud	combin14	–	–	–	–	450E+06	–
Lateral panel	solid45	1.55E+10	2300	0.17	–	–	–
Rail	beam4	2.056E+11	7850	0.3	–	–	–
Sleepers	mass21	–	–	–	290	–	–
K_{rs}	combin14	–	–	–	–	500E+06	–
C_{rs}	combin14	–	–	–	–	–	200E+03

Table 4
Comparison of eigenfrequencies from ambient measurements and numerical model

Mode	Frequency (Hz)	
	Experiment	Calculation
First vertical bending mode	4.14	4.15
First torsional mode	9.00	9.01
Second vertical bending mode	10.44	10.27
Second torsional mode	14.28	14.56

4. The dynamic train–bridge interaction model

The dynamic model for the train–bridge interaction system consists of the subsystem for the train and the subsystem for the bridge. The two subsystems are linked by coupling the displacement relationships between rail and wheel. A perfect contact between the wheel and the rail is assumed. Wheel hunting and track irregularities are not yet considered.

4.1. Train subsystem

The high-speed train considered in the vibration measurements is the Italian ETR500Y type. It is composed of a locomotive followed by eight passenger cars and another locomotive. The length of the locomotive is 19.7 m, while the length of the passenger car is 26.1 m. The average static axle loads for the locomotives and passenger cars are 176.4 and 112.9 kN, respectively.

The vehicle system, as commonly adopted in Refs. [15–18] is assumed as following (Fig. 12): each vehicle is considered as an independent entity with one car body, two bogies and four wheel sets. Both the primary and secondary suspension system can be simplified as an elastic system. The bogies and the wheel sets are linked by

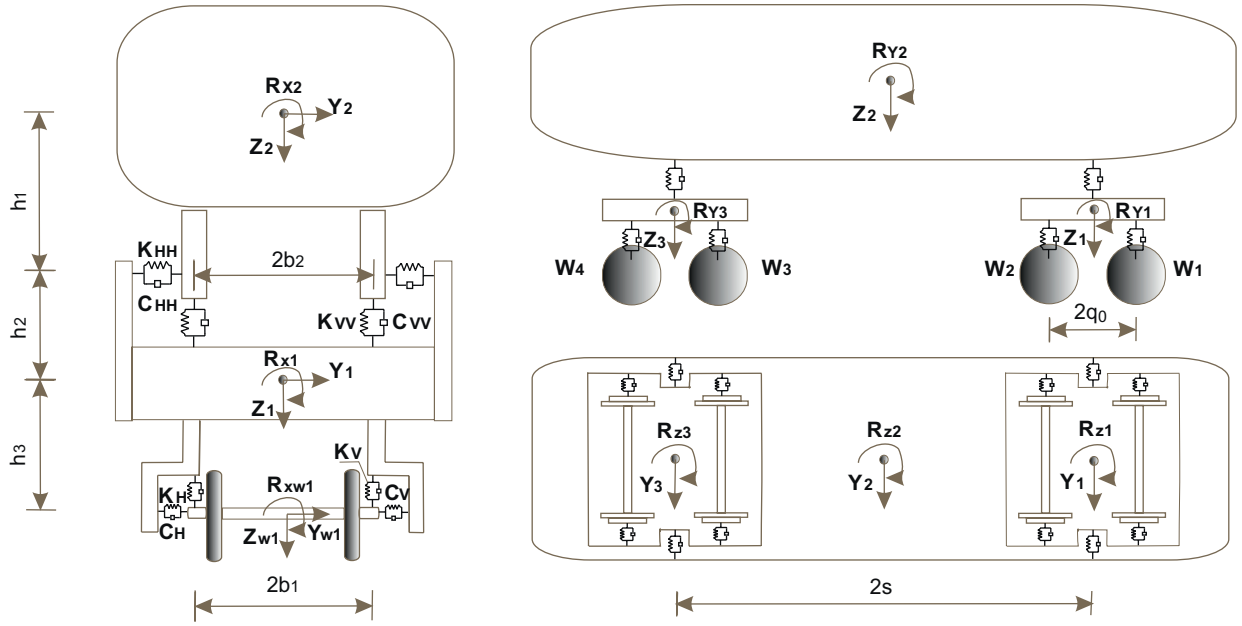

Fig. 12. Vehicle model.

horizontal and vertical springs and dampers. There are horizontal and vertical springs (K_H, K_V) and dampers (C_H, C_V) at each side of each wheel set, also horizontal and vertical springs (K_{HH}, K_{VV}) and dampers (C_{HH}, C_{VV}) at each side of each bogie. So in a vehicle there are eight horizontal and vertical springs and dampers in the primary suspending system, four horizontal and vertical springs and dampers in the secondary suspending system. Each car body and each bogie has 5 dof's: the displacement in vertical direction (Z) and longitudinal direction (Y), and rotations around the X-axis (R_X), Y-axis (R_Y) and Z-axis (R_Z). Each wheel set has 3 dof's: the displacement in vertical direction (Z) and longitudinal direction (Y), and rotation around the X-axis (R_X). In this way, the vehicle model has a degree of 27 dof's, in which the dof's of the wheel sets are linked to the movement of the bridge and only the remaining 15 ones are taken as independent dof's in the vehicle equations. The main characteristics of the train are listed in Table 5.

The displacement of a vehicle is defined by the following vector:

$$\mathbf{V}_v = \{Y_1, R_{X1}, R_{Z1}, Z_1, R_{Y1}, Y_2, R_{X2}, R_{Z2}, Z_2, R_{Y2}, Y_3, R_{X3}, R_{Z3}, Z_3, R_{Y3}\}^{\mathrm{T}}$$

where subscript 1 stands for the front bogie, subscript 2 stands for the car body and subscript 3 stands for the rear bogie.

The equation of motion of the vehicle can be expressed as

$$\mathbf{M}_v\ddot{\mathbf{V}}_v + \mathbf{C}_v\dot{\mathbf{V}}_v + \mathbf{K}_v\mathbf{V}_v = \mathbf{P}_v \tag{1}$$

where $\mathbf{M}_v$, $\mathbf{C}_v$ and $\mathbf{K}_v$ are mass, damping and stiffness matrices; $\mathbf{V}_v$, $\dot{\mathbf{V}}_v$ and $\ddot{\mathbf{V}}_v$ are the displacement, velocity and acceleration vectors of the vehicle system; $\mathbf{P}_v$ is the interaction force vector transferred to the bogies by the first suspension system [19].

For understanding the train–bridge interaction, it is useful to calculate the eigenfrequencies and eigenmodes of the vehicle.

Table 6 summarizes the eigenfrequencies and describes the corresponding mode shapes of the vehicle. The natural frequencies of the vehicle range from 0.26 to 6.06 Hz. The first bending frequency of 4 Hz of the bridge is in the range of natural frequencies of the vehicle. This can explain why the first bending frequency of the bridge is influenced when the train is on the bridge, while the second bending frequency remains almost unchanged. Fig. 13 shows the vertical modes of two bogies, which are very close to the first bending frequency of the bridge.

Table 5
Characteristics of ETR500Y high-speed train

Item	Unit	Locomotive	Passenger-car
Mass of car body (M_2)	kg	55,976	34231
Mass moment of inertia of car body around x-axis (I_{x2})	$kg \cdot m^2$	53,366	54642
Mass moment of inertia of car body around y-axis (I_{y2})	$kg \cdot m^2$	1,643,086	1,821,521
Mass moment of inertia of car body around z-axis (I_{z2})	$kg \cdot m^2$	1,630,520	1,760,619
Mass of bogie (M_1)	kg	3896	2760
Mass moment of inertia of bogie around x-axis (I_{x1})	$kg \cdot m^2$	3115	2304
Mass moment of inertia of bogie around y-axis (I_{y1})	$kg \cdot m^2$	5843	2504
Mass moment of inertia of bogie around z-axis (I_{z1})	$kg \cdot m^2$	8107	4071
Mass of wheel set (M_w)	kg	2059	1583
Mass moment of wheel set (I_w)	$kg \cdot m^2$	1164	753
Lateral stiffness of the primary suspension system (K_H)	kN/m	82,821	266,785
Vertical stiffness of the primary suspension system (K_V)	kN/m	896,100	404,370
Lateral damping of the primary suspension system (C_H)	$kN \cdot s/m$	0	0
Vertical damping of the primary suspension system (C_V)	$kN \cdot s/m$	7625	3750
Lateral stiffness of the secondary suspension system (K_{HH})	kN/m	73,035	32,054
Vertical stiffness of the secondary suspension system (K_{VV})	kN/m	236,030	90,277
Lateral damping of the secondary suspension system(C_{HH})	$kN \cdot s/m$	4625	5000
Vertical damping of the secondary suspension system (C_{VV})	$kN \cdot s/m$	18,125	8125
Half distance between two wheel-sets (q_0)	m	1.5	1.5
Half span of the primary suspension system (b_1)	m	1.115	0.965
Half span of the secondary suspension system (b_2)	m	1.0425	1.0825
Distance between the car body and the secondary suspension system (h_1)	m	0.915	0.7
Distance between the secondary suspension system and bogie (h_2)	m	0.098	0.12
Distance between the bogie and wheel sets (h_3)	m	0.087	0.13

Table 6
Computed natural frequencies of the vehicle

Mode	Frequeny (Hz)
Lateral and roll mode of the car body	0.2630
Anti-symmetrical lateral and roll mode of 2 bogies; yaw mode of the car body	0.3957
Symmetrical lateral and roll mode of 2 bogies; lateral and roll mode of car body	0.4709
Symmetrical vertical mode of 2 bogies, vertical mode of car body	0.4899
Anti-symmetrical vertical mode of 2 bogies, pitch mode of car body	0.6376
Symmetrical lateral and roll mode of 2 bogies	3.1963
Anti-symmetrical lateral and roll mode of 2 bogies	3.1969
Yaw mode of front bogie	3.8652
Yaw mode of rear bogie	3.8652
Symmetrical vertical mode of 2 bogies	4.0656
Anti-symmetrical vertical mode of 2 bogies	4.0680
Anti-symmetrical roll mode of 2 bogies	4.6691
Symmetrical roll mode of 2 bogies	4.6716
Pitch mode of front bogie	6.0676
Pitch mode of rear bogie	6.0676

4.2. Bridge subsystem

The equation of motion of the bridge can be expressed as

$$\mathbf{M}_b\ddot{\mathbf{V}}_b + \mathbf{C}_b\dot{\mathbf{V}}_b + \mathbf{K}_b\mathbf{V}_b = \mathbf{P}_b \tag{2}$$

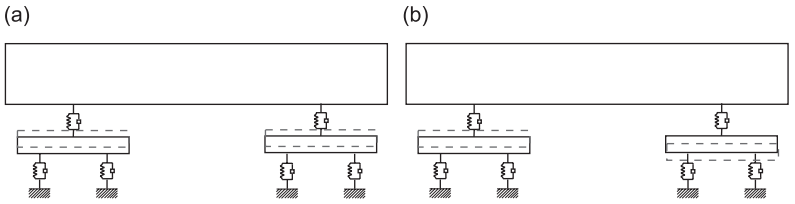

Fig. 13. Vertical modes of bogies: (a) symmetrical mode at 4.0656 Hz and (b) anti-symmetrical mode at 4.0680 Hz.

where $\mathbf{M}_b$, $\mathbf{C}_b$ and $\mathbf{K}_b$ are the mass matrix, damping matrix and stiffness matrix, respectively. $\mathbf{V}_b$, $\dot{\mathbf{V}}_b$ and $\ddot{\mathbf{V}}_b$ represent the displacement, velocity and acceleration vectors of the bridge, respectively. $\mathbf{P}_b$ is the force vector transferred to the bridge.

In the present numerical model developed for the Sesia viaduct, more than 8000 nodes and 11,000 elements are included. Therefore, the modal superposition method is adopted to solve the equation of the motion of the bridge. It is assumed that only the first N_0 modes of bridge are contributing to the interaction computation and the modal data are normalized to the mass matrix.

The displacements of the bridge can be expressed as

$$\mathbf{V}_b = \mathbf{\Phi} \cdot \mathrm{q} \tag{3}$$

where $\mathbf{\Phi}$ represents the first N_0 modes of bridge and $\mathbf{q}$ represents the displacement in modal coordinates.

Therefore the equation of motion of the bridge can be defined as follows:

$$\ddot{\mathbf{q}} + \mathbf{C}_b^* \dot{\mathbf{q}} + \mathbf{K}_b^* \mathbf{q} = \mathbf{P}_b^* \tag{4}$$

where $\mathbf{C}_b^*$, $\mathbf{K}_b^*$, $\mathbf{P}_b^*$ can be calculated by Eqs. (6), (5) and (7), respectively.

$$\mathbf{C}_b^* = \mathbf{\Phi}^{\mathrm{T}} \mathbf{C}_b \mathbf{\Phi} \tag{5}$$

$$\mathbf{K}_b^* = \mathbf{\Phi}^{\mathrm{T}} \mathbf{K}_b \mathbf{\Phi} \tag{6}$$

$$\mathbf{P}_b^* = \mathbf{\Phi}^{\mathrm{T}} \mathbf{P}_b \tag{7}$$

where $\mathbf{P}_b$ represents the force vector caused by the wheel–rail interaction. It is determined by position, movement status and mass of the wheel sets. The horizontal, torsional and vertical forces produced by wheel set i of bogie j corresponding to the deck displacement can be computed from the equilibrium displacement of the wheel:

$$\begin{cases} F_{YW1} = -M_{W1}\ddot{Y}_{W1} + 2C_H[\dot{Y}_1 + q\dot{R}_{Z1} - h_3\dot{R}_{X1} - \dot{Y}_{W1}] + 2K_H[Y_1 + qR_{Z1} - h_3R_{X1} - Y_{W1}] \\ F_{ZW1} = -M_{W1}\ddot{Z}_{W1} + 2C_V[\dot{Z}_1 + q\dot{R}_{Y1} - \dot{Z}_{W1}] + 2K_V[Z_1 + qR_{Y1} - Z_{W1}] + F_{G1} \\ F_{RXW1} = -I_{W1}\ddot{R}_{XW1} + 2C_V Db_1(\dot{R}_{X1} - \dot{R}_{XW1}) + 2K_V Db_1(R_{X1} - R_{XW1}) \end{cases} \tag{8}$$

$$\begin{cases} F_{YW2} = -M_{W2}\ddot{Y}_{W2} + 2C_H[\dot{Y}_1 + q\dot{R}_{Z1} - h_3\dot{R}_{X1} - \dot{Y}_{W2}] + 2K_H[Y_1 + qR_{Z1} - h_3R_{X1} - Y_{W2}] \\ F_{ZW2} = -M_{W2}\ddot{Z}_{W2} + 2C_V[\dot{Z}_1 + q\dot{R}_{Y1} - \dot{Z}_{W2}] + 2K_V[Z_1 + qR_{Y1} - Z_{W2}] + F_{G2} \\ F_{RXW2} = -I_{W2}\ddot{R}_{XW2} + 2C_V Db_1(\dot{R}_{X1} - \dot{R}_{XW2}) + 2K_V Db_1(R_{X1} - R_{XW2}) \end{cases} \tag{9}$$

$$\begin{cases} F_{YW3} = -M_{W3}\ddot{Y}_{W3} + 2C_H[\dot{Y}_3 + q\dot{R}_{Z3} - h_3\dot{R}_{X3} - \dot{Y}_{W3}] + 2K_H[Y_3 + qR_{Z3} - h_3R_{X3} - Y_{W3}] \\ F_{ZW3} = -M_{W3}\ddot{Z}_{W3} + 2C_V[\dot{Z}_3 + q\dot{R}_{Y3} - \dot{Z}_{W3}] + 2K_V[Z_3 + qR_{Y1} - Z_{W3}] + F_{G3} \\ F_{RXW3} = -I_{W3}\ddot{R}_{XW3} + 2C_V Db_1(\dot{R}_{X3} - \dot{R}_{XW3}) + 2K_V Db_1(R_{X3} - R_{XW3}) \end{cases} \tag{10}$$

$$\begin{cases} F_{YW4} = -M_{W3}\ddot{Y}_{W4} + 2C_H[\dot{Y}_3 + q\dot{R}_{Z3} - h_3\dot{R}_{X3} - \dot{Y}_{W4}] + 2K_H[Y_3 + qR_{Z3} - h_3R_{X3} - Y_{W4}] \\ F_{ZW4} = -M_{W3}\ddot{Z}_{W4} + 2C_V[\dot{Z}_3 + q\dot{R}_{Y3} - \dot{Z}_{W4}] + 2K_V[Z_3 + qR_{Y1} - Z_{W4}] + F_{G4} \\ F_{RXW4} = -I_{W3}\ddot{R}_{XW4} + 2C_V Db_1(\dot{R}_{X3} - \dot{R}_{XW4}) + 2K_V Db_1(R_{X3} - R_{XW4}) \end{cases} \tag{11}$$

where F_{YWi}, F_{ZWi}, F_{RXWi} ($i = 1, 2, 3, 4$) represent the forces and the moment under the ith wheel set. M_W is the mass of the wheel set, I_W is the inertia around the X-axis of the wheel set, F_G is the vehicle weight on the wheel and D is the gauge of the rail. The wheel–rail forces between nodes are transferred to the two neighboring rail nodes, which can be calculated by Eq. (12):

$$\begin{bmatrix} \mathbf{F}_{iN_1} \\ \mathbf{F}_{iN_2} \end{bmatrix} = \begin{bmatrix} \alpha_1 & 0 & 0 \\ 0 & \alpha_1 & 0 \\ 0 & 0 & \alpha_1 \\ \alpha_2 & 0 & 0 \\ 0 & \alpha_2 & 0 \\ 0 & 0 & \alpha_2 \end{bmatrix} \begin{bmatrix} F_{Yi} \\ F_{Zi} \\ F_{RXi} \end{bmatrix} \tag{12}$$

where N_1 and N_2 are the neighboring rail nodes of the ith wheel position; and $\mathbf{F}_{iN_1}$ and $\mathbf{F}_{iN_2}$ are the vectors of forces transferred to the nodes N_1 and N_2, respectively, F_{Yi}, F_{Zi}, F_{RXi} are the forces under the ith wheel. $\alpha_1 = d_2/(d_1 + d_2)$, $\alpha_2 = d_1/(d_1 + d_2)$, where d_1 and d_2 are the distances between the ith wheel position and the neighboring rail nodes N_1 and N_2, respectively.

In this paper, due to the high quality of the high-speed line, wheel hunting and track irregularities are not considered. The displacement of wheel set i under bogie j is taken equal to that of the same position on the structural member on which the vehicle runs.

4.3. Computation of the coupled train–bridge system

The vehicle subsystem and the bridge subsystem are linked by coupling the displacement relationships between wheel and rail [20]. As described before, the equations of motion of the vehicle subsystem and the bridge subsystem can be expressed as

$$\begin{cases} \mathbf{M}_v\ddot{\mathbf{V}}_v + \mathbf{C}_v\dot{\mathbf{V}}_v + \mathbf{K}_v\mathbf{V}_v = \mathbf{P}_v \\ \ddot{\mathbf{q}} + \mathbf{C}_b^*\dot{\mathbf{q}} + \mathbf{K}_b^*\mathbf{q} = \mathbf{P}_b^* \end{cases} \tag{13}$$

The displacements, velocities and accelerations of the vehicle and bridge system within a certain time step are computed in an iterative process shown in Fig. 14. The dynamic analysis of the bridge response due to the forces transmitted by the wheel is alternated with the dynamic analysis of the vehicle motion due to the bridge displacements. The integration of the equations is performed according to the Newmark-β method with value of $\beta = 0.25$ and $\gamma = 0.5$ according to the trapezoidal rule [21]. The rate of convergence is set as 0.001 for the acceleration response to assure the analytical accuracy.

4.4. Numerical prediction and comparison with measurements

According to the European standard [22], for the determination of the maximum deck acceleration, the frequencies in the dynamic analysis should be considered up to a maximum of: (i) 30 Hz; (ii) 1.5 times the frequency of the first mode shape of the structural element being considered, including at least the first three modes. For the Sesia viaduct, these two frequencies are 30 and 4.2 Hz. The threshold for low-pass filtering therefore is 30 Hz. The first 300 modes, with natural frequencies ranging from 2.78 to 40.37 Hz, are used for train–bridge interaction computation, with a uniform damping ratio equal to 2.5% for all modes. The speed of the train is set to 288 km/h according to the measurement. Fig. 15 shows the computed vertical displacement history of mid-span point 2b08 (see Fig. 3), the maximum displacement reaches 1.9 mm, which indicates that the Sesia viaduct is very stiff: for the train passage the maximum dynamic displacement is less than 2 mm with a span of about 45 m.

Figs. 16a and 17a compare the experimental and predicted time history of the vertical acceleration at points 2c06 and 2c12 (see Fig. 3) after a filtering to 30 Hz. A good agreement between the experimental and the predicted results is observed. The acceleration has approximately the same maximum value in the time domain. Figs. 16b and 17b depict the results in the frequency domain. A peak corresponding to the first

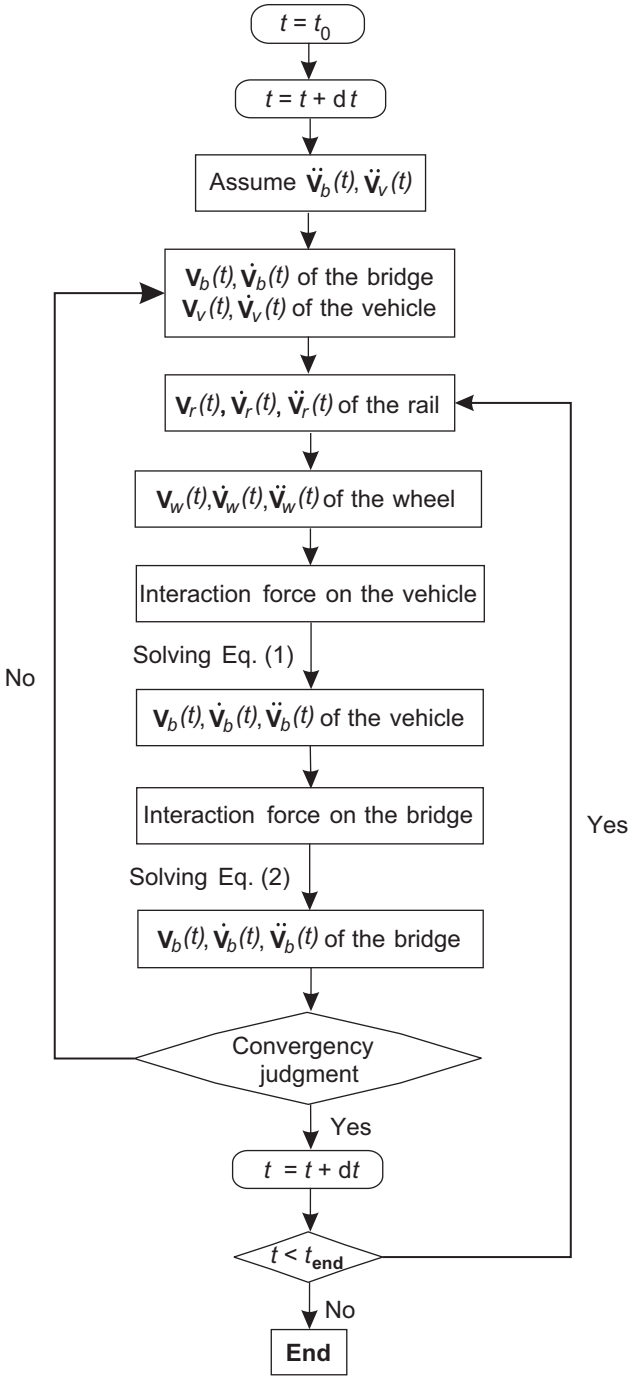

Fig. 14. Flowchart of solution procedure.

bending frequency of the bridge at 4 Hz is observed in the predicted as well as the measured spectra. The existing major peaks beyond 20 Hz are contributed by the higher modes, specifically the third torsional mode and the third bending mode. From the one-third octave band spectra (Figs. 16c and 17c), it can be seen that the correspondence between the predicted and experimental results is quite good, which indicates that the dynamic behavior of the bridge is properly estimated.

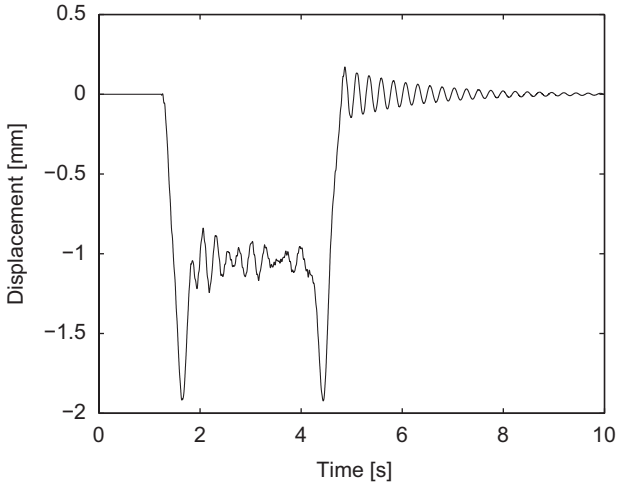

Fig. 15. Computed vertical displacement time history at point 2b08 (with train–bridge interaction model).

The predicted vertical acceleration of the car body is presented in Fig. 18. The low value of the vertical acceleration indicates that the inertial force is much lower than the train weights.

Fig. 19 compares the predicted and measured strain at point S16 (see Fig. 7). Both the prediction and the measurement almost have the same magnitude and the contribution of the axles can be clearly distinguished.

The force history in the stud is very meaningful as input for laboratory fatigue tests and fatigue analysis. In the numerical model, the spring element combin14 is chosen to represent the shear studs that connect the flanges with the concrete slab. Fig. 20 shows a typical force time history in one stud.

The passage of successive loads with uniform spacing can excite the structure in resonance when critical speed is reached. Fig. 21 shows the predicted maximum displacement of mid-span point 2b08 under varying train speeds. Computations are made in the interval [250,400] km/h with a step of 5 km/h. The resonance speed is reached at 380 km/h.

The critical speed can also be computed as follows [2]:

$$V_{\mathrm{cri}} = \frac{l_0}{i} \times f_n, \quad i = 1, 2, 3, \ldots, n \tag{14}$$

For Italian high-speed train ETR500Y, $l_0 = 26.1$ m, $i = 1$, and $f_1 = 4.15$ Hz, The critical speed is 389 km/h, which matches well with the train–bridge interaction analysis.

5. Moving load model

Another alternative for predicting the bridge response under train passages is using a series of moving loads to represent the effects of the moving train.

The distribution of n vertical axle loads moving in the longitudinal y direction is written as the summation of the product of Dirac functions that determine the time-dependent position $\mathbf{x}_k = \{x_{k0}, y_{k0} + vt, z_{k0}\}^{\mathrm{T}}$. The time history $g_{sk}(t)$ of the constant load is equal to the kth axle weight of the train [23]:

$$P_{bk}(\mathbf{x}, t) = \sum_{k=1}^{n} \delta(x - x_{k0})\delta(y - y_{k0} - vt)\delta(z - z_{k0}) g_{sk}(t)\mathbf{e}_z \tag{15}$$

y_{k0} is the initial position of the kth axle that moves with the train speed v along the y-axis and $\mathbf{e}_z$ denotes the vertical unit vector.

Fig. 22 depicts the predicted time history and frequency content of the vertical acceleration at point 2c12 (see Fig. 3) after a filtering to 30 Hz. It can be again concluded that, there is a good match between the experimental and numerical predictions as well. Fig. 23 shows the very small difference of the predicted

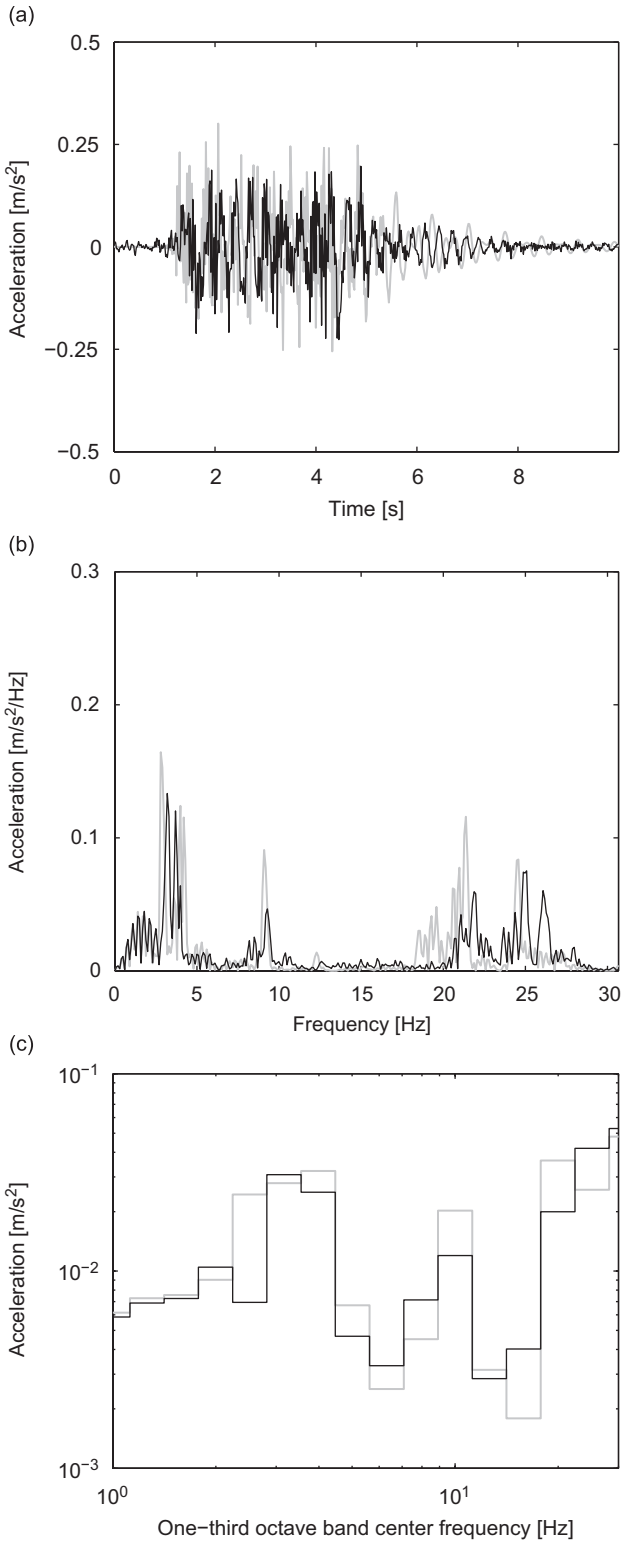

Fig. 16. Comparison of acceleration at point 2c06 between prediction (gray line, with train–bridge interaction model) and measurement (black line): (a) time history, (b) frequency content and (c) one-third octave band RMS spectra.

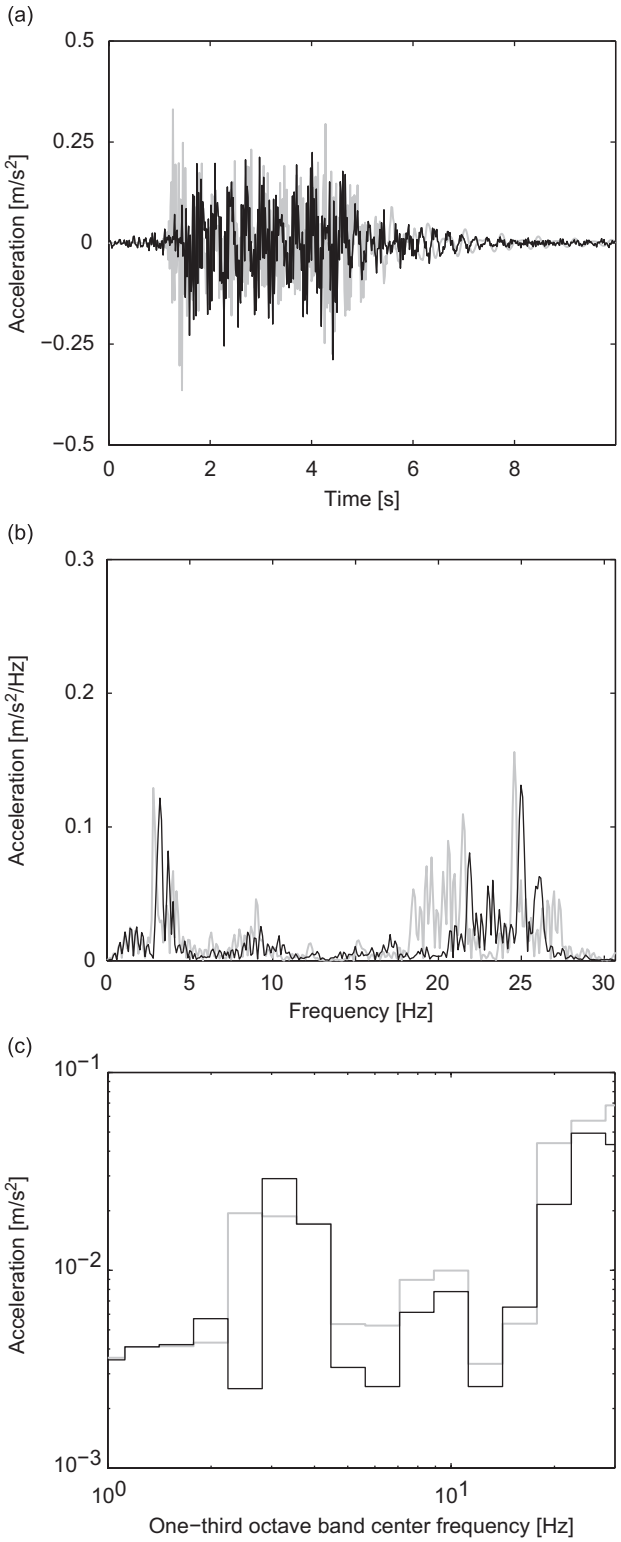

Fig. 17. Comparison of acceleration at point 2c12 between prediction (gray line, with train–bridge interaction model) and measurement (black line): (a) time history, (b) frequency content and (c) one-third octave band RMS spectra.

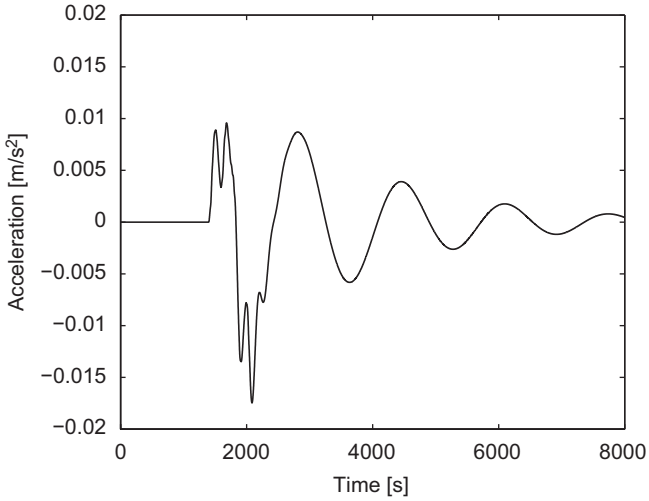

Fig. 18. Vertical acceleration of the car body.

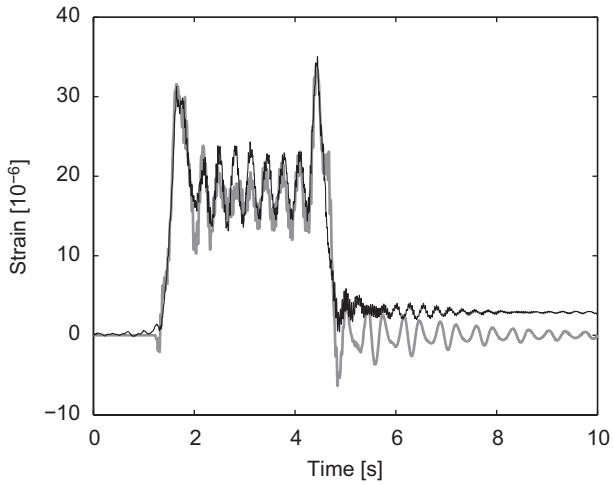

Fig. 19. Comparison of predicted strain histories (gray line, with train–bridge interaction model) with measured ones (black line) at point S16.

acceleration at point 2c12 between the two models in the frequency domain. A peak occurs at 4 Hz which confirms the interaction behavior between the vehicle and bridge, however, the interaction effect is so small that the interaction effect can be neglected. This is due to the high stiffness of the bridge and therefore the inertia effect and the interaction effects of the suspended vehicle systems are very small. Furthermore, the rails of the high-speed line have a quite good quality so that the wheel mass effects do not play an important role. The conclusion can be drawn that as far as the bridge response is concerned, the simple moving load model gives excellent results and is by far more efficient compared to the expensive computation of the train–bridge interaction model. However, if the response of the vehicle is of interest, the train–bridge interaction model should be preferred.

6. Conclusions

The main objective of this paper is to present the dynamic experiments of the Sesia viaduct and the experimental validation of two numerical prediction methods for estimating the vibrations of the bridge due to

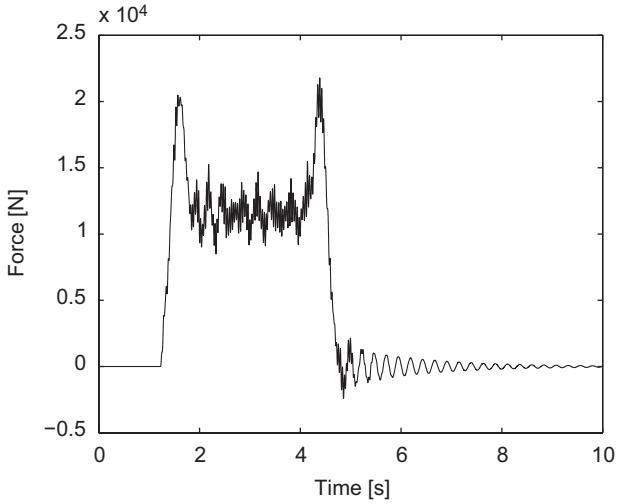

Fig. 20. Typical force time history in one stud (with train–bridge interaction model).

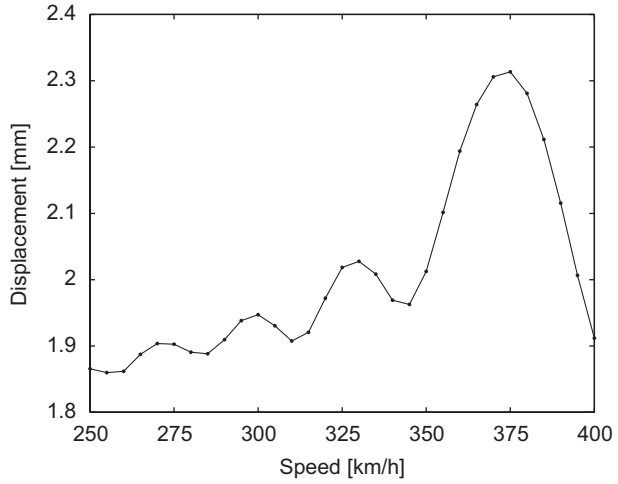

Fig. 21. Maximum displacement at point 2b08 under varying train speeds (with train–bridge interaction model).

a train passage. For the dynamic experiments, not only accelerations are measured but also axial strains by fiber optical sensors. Based on the dynamic behavior of the adjacent spans, the modes of the bridge can be approximately distinguished as symmetrical and anti-symmetrical patterns, which indicates that, although each span is statically decoupled, the ballast and the rails realize a connection between neighboring spans. The symmetrical modes are predominantly excited when the train passes bridge. Therefore, the numerical model is developed according to the symmetrical modal properties, i.e. appropriate boundary conditions are applied in the longitudinal direction of the rail and the ballast to simulate their continuity.

Two approaches for predicting bridge responses under the excitation of train are adopted: the train–bridge interaction model and the moving load model. Both models give a good match of the response with the experiment. The results suggest that the moving load model allows for an accurate prediction of the bridge response and is by far more efficient. However, if the response of the vehicle is of interest, the train–bridge interaction model should be preferred.

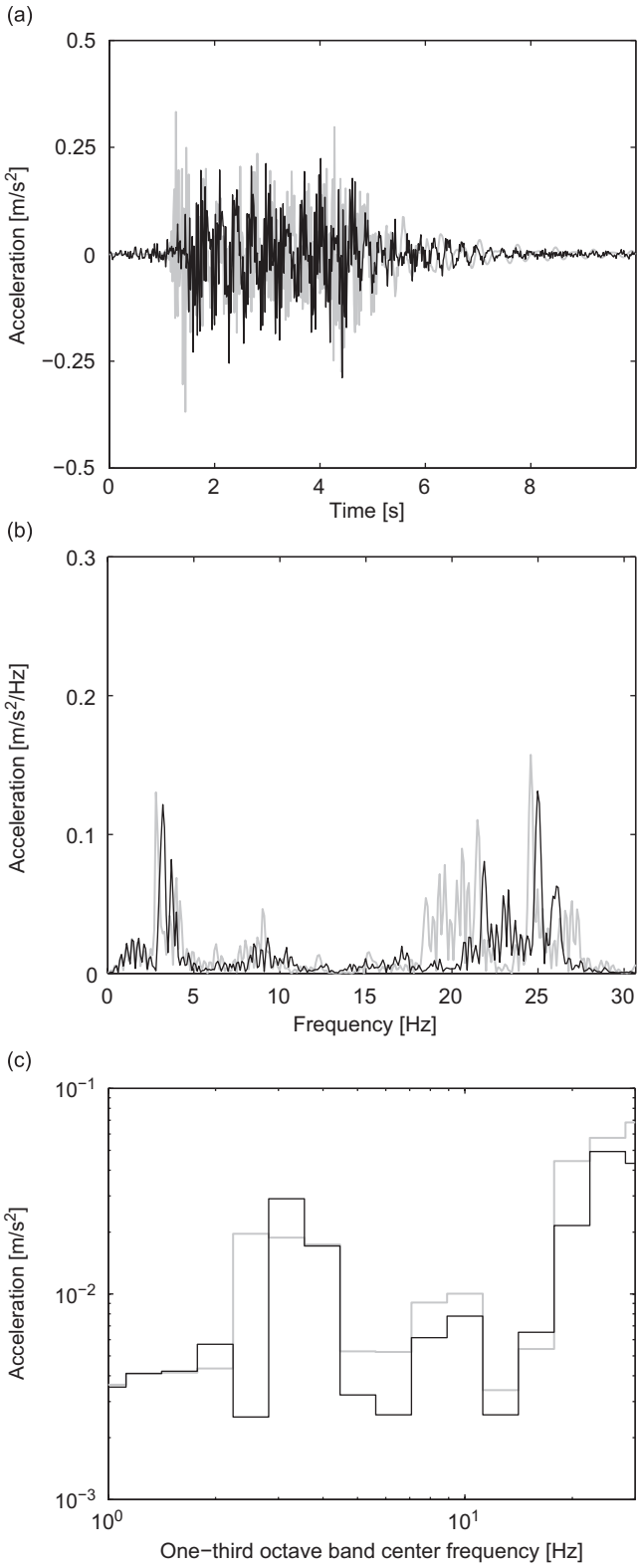

Fig. 22. Comparison of acceleration at point 2c12 between prediction (dash line, with moving load model) and measurement (solid line): (a) time history, (b) frequency content and (c) one-third octave band RMS spectra.

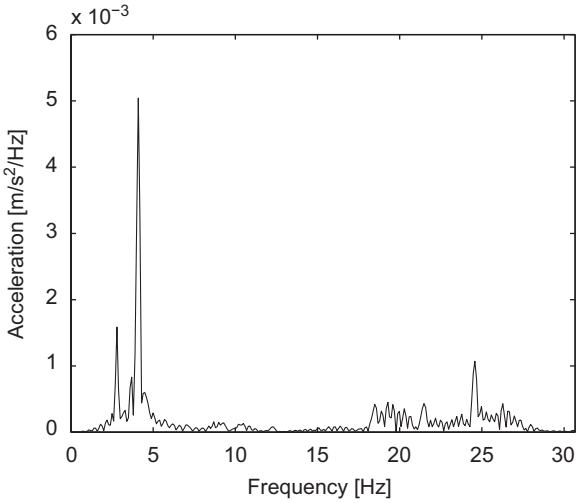

Fig. 23. Difference of the predicted acceleration at point 2c12 in the frequency domain between the train–bridge interaction model and the moving load model.

This study also allows a better understanding of the structural behavior of the composite railway bridge. From these measurements and the modeling application, it can be concluded that using proper equipment and suitable layouts of sensors, the dynamic behavior of bridges can be assessed by vibration measurements, opening the way for continuous health monitoring.

Acknowledgments

The research is conducted in the framework of the EC Research Fund for Coal and Steel RTD project RFSR-CT-2006-00032 "DETAILS" (Design for optimal life cycle costs (LCC) of high-speed railway bridges by enhanced monitoring systems). The support of the EC is gratefully acknowledged.

References

[1] Steel RTD proposal: design for optimal life cycle costs (LCC) of high-speed railway bridges by enhanced monitoring systems, September, 2005.
[2] L. Frýba, Vibration of solids and structures under moving loads, *Thomas Telford* (1999).
[3] X. Zhang, K. Sennah, J.B. Kennedy, Evaluation of impact factors for composite concrete–steel cellular straight bridges, *Engineering Structures* 25 (2003) 313–321.
[4] Y.B. Yang, J.D. Yau, L.C. Hsu, Vibration of simple beams due to trains moving at high-speeds, *Engineering Structures* 19 (1997) 936–944.
[5] G. De Roeck, J. Maeck, A. Teughels, Train–bridge interaction validation of numerical models by experiments on high-speed railway bridge in Antoing, TIVC'2001, Beijing, 2001.
[6] J.Z. Li, M.B. Su, The resonant vibration for a simply supported girder bridge under high-speed trains, *Journal of Sound and Vibration* 224 (1999) 897–915.
[7] C.W. Kim, M. Kawatani, K.B. Kim, Three-dimensional dynamic analysis for bridge–vehicle interaction with roadway roughness, *Engineering Structures* 83 (2005) 1627–1645.
[8] G. Diana, F. Cheli, Dynamic interaction of railway systems with large bridges, *Vehicle System Dynamics* 18 (1989) 71–106.
[9] M.K. Song, H.C. Nohb, C.K. Choi, A new three-dimensional finite element analysis model of high-speed train–bridge interactions, *Engineering Structures* 25 (2003) 1611–1626.
[10] C.H. Lee, C.W. Kim, M. Kawatani, N. Nishimura, T. Kamizono, Dynamic response analysis of monorail bridges under moving trains and riding comfort of trains, *Engineering Structures* 27 (2005) 1999–2013.
[11] H. Xia, N. Zhang, G. De Roeck, Dynamic analysis of high-speed railway bridge under articulated trains, *Computers and Structures* 81 (2003) 2467–2478.
[12] B. Peeters, G. De Roeck, Reference-based stochastic subspace identification for output-only modal analysis, *Mechanical Systems and Signal Processing* 13 (1999) 855–878.

[13] F.D. Queiroz, P.C.G.S. Vellasco, D.A. Nethercot, Finite element modelling of composite beams with full and partial shear connection, *Journal of Constructional Steel Research* 63 (2007) 505–521.
[14] C. Odenbreit, A. Leffer, M. Feldmann, Fatigue behavior of shear studs to transfer dynamic loads between steel and concrete construction elements, Sea Tech Week-fatigue of Maritime Structures, Brest, 2004.
[15] Y.K. Cheung, F.T.K. Au, D.Y. Zheng, Y.S. Cheng, Vibration of multi-span bridges under moving vehicles and trains by using modified beam vibration functions, *Journal of Sound and Vibration* 228 (1999) 611–628.
[16] H. Xia, Y.L. Xu, T.H.T. Chan, Dynamic interaction of long suspension bridges with running trains, *Journal of Sound and Vibration* 237 (2000) 263–280.
[17] C.H. Lee, M. Kawatani, C.W. Kim, N. Nishimura, Y. Kobayashi, Dynamic response of a monorail steel bridge under a moving train, *Journal of Sound and Vibration* 294 (2006) 562–579.
[18] N. Zhang, H. Xia, W.W. Guo, Vehicle–bridge interaction analysis under high-speed trains, *Journal of Sound and Vibration* 309 (2008) 407–425.
[19] K. Liu, E. Rynders, G. De Roeck, Experimental validation of the dynamic interaction analysis between high-speed trains and the Sesia viaduct, IMAC26, Orlando, 2008.
[20] Q.L. Zhang, Q. Vrouwenvelder, J. Wardenier, Numerical simulation of train–bridge interactive dynamics, *Computers and Structures* 79 (2001) 1059–1075.
[21] N.M. Newmark, A method of computation for structural dynamics, *Journal of Engineering Mechanics* 96 (1970) 593–620.
[22] EN 1990:2002/A1:2005, Eurocode—Basis of structural design, Final Draft. European Committee for standardization, CEN, 2006.
[23] G. Lombaert, G. Degrande, J. Kogut, S. François, The experimental validation of a numerical model for the prediction of railway induced vibrations, *Journal of Sound and Vibration* 297 (2006) 512–535.